Review

Tungsten Disulfide-Based Materials and Their Conjugates for Cancer Photothermal Therapy

Ana R. Lopes , Fernão D. Magalhães , Joana A. Loureiro , Artur M. Pinto *

Posted Date: 15 October 2024

doi: 10.20944/preprints202410.1155.v1

Keywords: Tungsten disulfide (WS2); Photothermal therapy (PTT); Photodynamic therapy (PDT); Biocompatibility; Drug delivery; Cancer treatment

Review

Tungsten Disulfide-Based Materials and Their Conjugates for Cancer Photothermal Therapy

Ana Rita Lopes [1,2], Fernão D. Magalhães [1,2], Joana A. Loureiro [1,2,3] and Artur M. Pinto [1,2,*]

[1] LEPABE – Laboratory for Process Engineering, Environment, Biotechnology and Energy, Faculty of Engineering, University of Porto, Rua Dr. Roberto Frias, 4200-465 Porto, Portugal
[2] ALiCE – Associate Laboratory in Chemical Engineering, Faculty of Engineering, University of Porto, Rua Dr. Roberto Frias, 4200-465 Porto, Portugal
[3] Department of Metallurgical and Materials Engineering, Faculty of Engineering, University of Porto, Rua Dr. Roberto Frias, 4200-465 Porto, Portugal
* Correspondence: arturp@fe.up.pt

Abstract: Cancer remains one of the most critical global health issues. Conventional treatments, such as radiotherapy, surgery, or chemotherapy, have limitations, especially concerning side effects, resistance, and recurrence. Consequently, new innovative treatments to overcome these problems are needed. Photothermal therapy (PTT) is a promising alternative that uses photothermal agents that convert near-infrared light (NIR) into heat to kill cancer cells. Nanoparticles can be used as photothermal agents and also as drug delivery platforms, improving the drugs' stability, allowing for targeted delivery, and reducing toxicity. Due to its broad absorption band, high surface area, and versatility for surface functionalization, tungsten disulfide (WS_2) has high potential in this context. This paper presents the state-of-the-art on the use of WS_2-based materials to achieve effective and biocompatible anti-anticancer new treatment strategies.

Keywords: Tungsten disulfide (WS_2); Photothermal therapy (PTT); Photodynamic therapy (PDT); Biocompatibility; Drug delivery; Cancer treatment

1. Introduction

Cancer is one of the biggest world health issues, leading the way for a huge number of deaths worldwide. In 2020, 19.3 million new cases of cancer were reported worldwide, from which about 10 million resulted in death. World Health Organization estimates reveal 28.9 million new cases by 2040, and 16.2 million deaths per year [1]. Radiotherapy is the most used treatment for cancer in combination with surgery, immunotherapy, and chemotherapy. However, this treatment is limited by the radiation that can be emitted, due to not harming the healthy cells around the cancer ones. So, there is an urge to find new ways to target only the tumor cells while not damaging the healthy ones around [2].

As an alternative to more conventional treatments, photothermal and photodynamic therapy (PDT) with nanoparticles have been gaining more attention. Photothermal therapy (PTT) uses agents that are administered at the tumor site that absorb near-infrared (NIR) light from a light source (e.g., laser), converting it to heat [3]. Photodynamic therapy uses photosensitizers (PS) that, when exposed to light, produce reactive oxygen species (ROS) that will kill tumor cells [4]. Even though PTT and PDT hold great value for the treatment of cancer, there are still issues to be addressed regarding the use of laser devices that can harm normal tissues, the body absorption/distribution, toxicity, and water stability of phototherapeutic agents used, and the heat resistance of some types of cancer cells [5]. Using nanomaterials as PTT agents not only improves the photothermal efficiency but also reduces the risks associated with the treatment. Different nanoparticles have been studied for these treatments since they possess good physicochemical and optical absorption properties. Furthermore, surface modifications can be performed with other molecules, improving their water stability, biocompatibility, and selectivity [6]. PTT and chemotherapy show great synergy. The increase in

 doi:10.20944/preprints202410.1155.v1

temperature caused by PTT enhances the cellular uptake and release of the chemotherapeutic drugs in the tumor. The introduction of 2D nanomaterials in PTT improves this synergy by providing a platform for drug delivery due to their large surface area and the possibility of surface modifications [7].

Several types of 2D nanomaterials have been tested for PTT, such as graphene-based materials (GBM), transition metal dichalcogenides (TMDCs), transition metal oxides (TMOs), transition metal carbides, nitrides and carbonitrides (MXenes), black phosphorus (BP), and others. Those can be produced through different routes based on top-down or bottom-up approaches. The top-down methods involve the breaking of bulk materials into smaller particles through mechanical and/or liquid exfoliation methods. These methods essentially implicate the breaking of the Van der Waals interactions between the layers of the bulk material. On the other hand, the bottom-up approaches involve the synthesis of nanomaterials from the atomic or molecular level into larger structures. Chemical-based methods are often used, such as chemical vapor deposition and wet-chemical synthesis [8].

Graphene is composed of one thin layer of carbon atoms arranged in a honeycomb lattice. Graphene nanoparticles present unique properties, such as a large surface area, planar and thin shape, high thermal (5000 W m^{-1} K^{-1}), and electrical conductivity. Furthermore, it has good mechanical and optical properties, and a high extinction coefficient in the near-infrared range (NIR), which makes graphene a good photothermal agent [9,10]. Different types of graphene-based materials can be obtained using different production/modification methods [11,12]. Transition metal oxides (TMOs) are composed of metals bound to oxygen atoms, in single or multilayer, where the oxygen atom polarizes the transition metal's electrons. Due to this strong polarization, planar TMOs show large non-linear and non-uniform distribution charges, that leads to extraordinary local surface and interfacial properties [13]. TMOs have good optical properties, and high surface-to-volume ratio. Furthermore, TMOs can interact directly with biomolecules through surface modification, making them suitable for drug delivery or cancer therapy [14]. MnO_2 is the most commonly studied TMO [15]. MXenes include transition metal carbides, nitrides, and carbonitrides. The generic formula for MXenes is $M_{n+1}X_n$, where M represents an early transition metal and X represents carbon or nitrogen [16]. MXenes surface can be modified with hydroxyls, oxygen, or fluorine, which makes them stable in aqueous media, improves biocompatibility, and allows conjugation with other molecules [17]. Another interesting 2D nanomaterial is black phosphorus (BP), a single layer of phosphorus atoms arranged in a honeycomb-like lattice structure. The tunable band gap, good thermal and optical properties, and nontoxic degradation products make this material suitable for biomedical applications [18]. Other nanomaterials, such as Palladium (Pd) nanoparticles have been investigated for PTT applications due to their high photothermal conversion efficiency, high NIR absorption, and excellent photothermal stability and biocompatibility [19]. Layered double hydroxides (LDHs) have also gained more attention due to their biocompatibility, tunable chemical composition, and the ability to exchange intercalated anions [20].

Transition metal dichalcogenides (TMDCs) are composed of transition metals inserted into layers of chalcogen atoms. TMDCs have a generic formula of MX_2, where M represents the transition metal and X is the chalcogen. The transition metals are positioned between two chalcogen (X) atoms layers, linked by weak van der Waals interactions [21]. TMDCs can be produced through various methods, such as mechanical exfoliation, liquid phase exfoliation, chemical exfoliation, solvothermal synthesis or chemical vapor deposition [22]. TMDCs present singular properties, especially their cytocompatibility, versatile surface chemistry and high photothermal conversion, making them suitable to be used as photothermal agents and in drug delivery applications [6]. TMDCs have a broad absorption in the NIR region because of their small band gap, which allows them to absorb light in this region while having a high photothermal conversion efficiency, which enables the use of lower power density NIR sources [23]. Also, because of their versatile surface chemistry, surface functionalization can be done with polymers or surfactants, to improve dispersibility, stability and biocompatibility [23]. Molybdenum disulfide (MoS_2) is the most researched TMDC, followed by WS_2

 doi:10.20944/preprints202410.1155.v1

and $MoSe_2$. In vitro studies with MoS_2 have been published for the first time in 2013, demonstrating its potential as a photothermal agent [24].

WS_2 nanoparticles consist of sheets of tungsten atoms sandwiched between layers of sulfur atoms. WS_2 can be produced via either top-down or bottom-up approaches. For the top-down methods, since the interlayer Van der Waals' force of the bulk material is weak, 2D nanosheets can be produced from their initial bulk materials, through various types of exfoliation, such as mechanical, liquid-based, alkalis-based, ion-intercalation, or electrochemical methods. Mechanical exfoliation is based on the adhesion of adhesive tape and bulk crystal to obtain monolayer or few-layer nanosheets. As for liquid-phase exfoliation, this method is based on the ultrasonication of bulk crystals in a solvent. The waves resulting from ultrasonication propagate through the solvent, causing the weaker Van der Waals interactions to break. Chemical exfoliation methods can also be used to produce ultrathin nanosheets. In this method, species are inserted between the interlayer cavity, expanding its distance and weakening the interactions between each layer. Lithium is the most used species in intercalation, due to its reaction with water, which produces hydrogen gas that, through its expansion, allows the separation of the nanosheet's layers [22,25]. On the other hand, bottom-up production can also be used, with methods such as chemical vapor deposition (CVD) or hydro-/solvothermal synthesis being the most common [26]. CVD refers to the reaction of a metal and a chalcogen with precursors under high temperature and pressure, resulting in ultrathin nanosheets. In the solvothermal method, a precursor under specific solvent conditions and specific reaction time is used to obtain the materials [22,25]. WS_2 has a large specific surface area and many active sites on the surface, which makes surface functionalization easier. Furthermore, WS_2 has a big adsorption band, having good absorption from ultraviolet to infrared regions. These features enable its use for drug delivery and cancer PTT [27].

Despite all the above-mentioned advantages, WS_2 still faces some problems, such as poor stability in physiological conditions, low biocompatibility at high concentrations, and low cellular uptake efficiency. Different types of surface modification have been used to overcome this problem, such as using polyethylene glycol (PEG) or bis(trimethylsilyl)acetamide (BSA). These coatings not only enhance the stability and dispersibility of the WS_2 nanosheets in physiological environments but can also improve cellular uptake in cancer cells. Also, improving the PTT effect and drug-loading efficiency [28].

2. Functionalization of WS_2 Nanoparticles

Surface functionalization can be performed by covalent or non-covalent interactions. In covalent functionalization, a chemical bond is formed between the nanomaterial and the functional compounds. One type of covalent functionalization is chemical oxidation, where oxygen groups like carboxyls (-COOH), epoxides (-C-O-C) and hydroxyls (-OH) are introduced at nanomaterials' surface [6]. Another example is the introduction of PEG molecules (PEGylation), from the reaction with nanomaterials' carboxyl groups, for example, which usually results in improved stability in physiological media and biocompatibility [29]. However, this type of process can lead to changes in nanomaterials' structure and key properties, for example, by disrupting delocalized π–π bonds, which can cause a decrease in photothermal conversion efficiency, affecting their application in PTT. Therefore, sometimes, non-covalent functionalization is more suitable. Non-covalent modifications are based on surface interaction with other molecules through Van der Waals forces, π–π stacking, hydrophobic/hydrophilic interactions, electrostatic forces, hydrogen bonding, and ionic and coordination bonds. These interactions can be often reversed and are usually weaker than covalent ones. [30]

Several strategies have been successfully developed to functionalize WS_2 (**Table 1**). WS_2 can be conjugated with polymers, such as PEG, BSA and PVP, or other inorganic or organic molecules, for example, liposomes. PEG is one of the most used polymers for WS_2 surface modification. Xie et al. [28] proved that the photothermal properties of WS_2 were improved using the thiol chemistry to functionalize WS_2 surface with PEG. After 5 min of NIR irradiation (808 nm laser, 0.8 W cm^{-2}), a concentration-dependent increase of WS_2-PEG temperature was found. The mass extinction

 doi:10.20944/preprints202410.1155.v1

coefficient at 808 nm measured was 23.8 L g^{-1} cm^{-1}, higher than graphene oxide (3.6 L g^{-1} cm^{-1}) and similar to rGO (24.6 L g^{-1} cm^{-1}) [31]. These results suggest that WS_2-PEG can be a strong photothermal agent for PTT. WS_2 functionalized with iron oxide (IO) nanoparticles at the surface, using a solvothermal method, coated with mesoporous silica (MS), and further functionalized with PEG, WS_2-IO-MS-PEG, was loaded with DOX by mixing both solutions for 24h at room temperature in PBS (pH 8), resulting in WS_2-IO-MS-PEG/DOX. This nanoparticle demonstrated improved stability in water, saline, and serum media, without any agglomeration observed up to 24 h. TEM imaging showed a mesoporous silica shell, with a thickness of 10 nm, on the surface of WS_2-IO-MS, while BET measurements determined a high surface area of 568.03 m^2 g^{-1}, which favors effective drug loading and release. The mass extinction coefficient, at 800 nm, was 23.8 L g^{-1} cm^{-1}, the same as for WS_2-PEG above mentioned [28]. WS_2-IO-MS-PEG also showed excellent photothermal stability, upon 5 cycles of 808 nm laser irradiation (0.8 W cm^{-2}, 3 min each cycle) [32]. Yi et al. [33] studied the functionalization of WS_2 with BSA by electrostatic surface adsorption. This functionalization improved the stability in water, saline or DMEM media. The photothermal conversion capability of WS_2-BSA was also tested for different concentrations and laser power densities. With the increase of concentrations and laser power, temperatures achieved also increased. As an example, when a concentration of 50 ppm WS_2-BSA, at T = 26 °C, was irradiated (1.5 W cm^{-2}, 808 nm), a temperature of 44.5°C was reached within 5 min. Furthermore, WS_2-BSA showed good photothermal stability. An innovative WS_2 nanosheet derived from Fe(III) species and modified with PVP on the surface, produced by a solvothermal method, was tested for stability in different media, such as water, saline and DMEM, and did not show any meaningful changes after 24 h. In addition, the biodegradation rate was also studied, and it could be seen that it increased quickly due to the presence of the Fe(III) species. The mass extinction coefficient of Fe(III)@WS_2-PVP was calculated to be 3.4 L g^{-1} cm^{-1}, lower than other WS_2 (only) nanoparticles but similar to graphene oxide (3.6 L g^{-1} cm^{-1}). The photothermal conversion capability of these nanoparticles was also tested using different concentrations and power laser densities. For a concentration of 200 μg mL^{-1}, upon NIR laser irradiation (5 min, 808 nm laser, 1 W cm^{-2}), a temperature of 45°C was reached [34].

Organic molecules, such as liposomes, can also be used for surface modification WS_2 can be conjugated with liposomes by electrostatic adsorption, which improves not only the stability in water and other media but can also improve the drug delivery inside the cells and the biocompatibility of the nanoparticles. In a study, WS_2-lipid (200 μg mL^{-1}) reached a temperature of 60 °C after 10 min of NIR irradiation (808 nm laser, 2 W cm^{-2}) [35]. Xie et al. [36] developed iron oxide-loaded WS_2 (m-WS_2) modified with lipids. Iron oxide was loaded onto the WS_2 surface by the solvothermal method and lipids, were mixed at 37 °C for 24h, resulting in mWS_2-lipid nanoparticles. After 10 min of NIR irradiation (808 nm laser, 2 W cm^{-2}), mWS_2-lipid reached 60.7 °C. WS_2/Au-lipid, gold doped WS_2, produced through a sodium citrate reduction method and modified with lipids, by the method previously described, reached 65 °C, under the same irradiation conditions [37]. Apart from previously mentioned functionalization strategies, there are other methods to produce innovative WS_2 nanoparticles, with unique characteristics. For example, the production of 1T-WS_2 ultrathin nanosheets through a hydrothermal reaction created nanosheets with good biocompatibility and photostability, exhibiting a strong absorption in the NIR region. These NPs were highly hydrophilic and presented great dispersibility in water, with no agglomeration, even after 1 year. They also showed good photothermal conversion capability, with temperature increments of 34 °C within 5 min, under 808 nm laser irradiation (0.6 W cm^{-2}) [38].

The doping of WS_2 nanosheets' surface with elements is another strategy that can be used to improve their properties. The doping of WS_2 with gadolinium, Gd^{3+}, and further modification with PEG, resulted in stable NPs in PBS, 1640-Medium, and fetal bovine serum (FBS), with improved photothermal characteristics. After 5 min of NIR irradiation (808 nm laser, 0.8 W cm^{-2}), the NPs also showed a concentration-dependent temperature increase. The mass extinction coefficient of WS_2:Gd^{3+}-PEG was 22.6 L g^{-1} cm^{-1}, slightly lower than for WS_2-PEG and WS_2-IO-MS-PEG [39]. Ying et al. [40] developed a PEGylated WS_2 (W) delivery system of DOX (D), which was adsorbed to the surface of the NPs in conjunction with ICG (I), a medical contrast agent, that under NIR laser

 doi:10.20944/preprints202410.1155.v1

irradiation can produce ROS and hyperthermia in PDT/PTT therapy. This system was then coated with DSPE-PEG-2000-FA-modified erythrocyte membrane (M-FA) to produce WID@M-FA NPs. The modification improved cell-targeting ability of the nanocarrier through FA receptor interactions. WID@M-FA NPs showed great photothermal properties, reaching 60 °C after 5 min of 808 nm laser irradiation (1 W cm^{-2}), while showing good photothermal stability.

Table 1. Tungsten disulfide functionalization and drug conjugation strategies.

Material produced	Drug conjugation	Method	Physicochemical properties alteration	Reference
WS_2 - BSA	-	1) WS_2 production by ultrasound-assisted liquid phase exfoliation 2) BSA electrostatic adsorption on the surface by stirring	Improved stability in saline, water and DMEM Zeta potential: BSA = −27.4 mV WS_2 = 20.8 mV WS_2-BSA = −19.8 mV	[33]
Fe (III)-WS_2 - PVP	DOX Drug loading: 41% (Fe (III)-WS_2 -PVP: DOX weight ratio: n/s) Drug release: 7.5 (pH 7.4; 6 h) 12.7% (pH 7.4; 48 h) 37% (pH 6.0; 6 h) 48.2% (pH 6.0; 48 h)	1) Fe (III)- WS_2 - PVP formation by hydrothermal reaction 2) DOX adsorption on Fe (III)- WS_2 - PVP	Increased biodegradation rate Improved stability in saline, water and DMEM	[34]
WS_2 – PEG	-	Covalent bond formation between WS_2 and PEG	Improved stability in saline Improved photothermal properties: broad NIR absorption band 700-1000 nm	[28]
WID-M-FA	DOX loading: 24.2% (WID-M-FA: DOX weight ratio: n/s)	1) LA-PEG_{2000}-NH_2 adsorption on WS_2 surface 2) WI formation through non-	Improved water stability and biocompatibility. Improved photothermal properties: higher absorption at 808 nm.	[40]

 doi:10.20944/preprints202410.1155.v1

	DOX release: 12 % (pH 7.4; 20 h) 30.9% (pH 7.4; 72 h) 24.2% (pH 5.2; 20 h) 56.4% (pH 5.2; 72 h) ICG loading: 22.9% (WID-M-FA: ICG weight ratio: n/s) ICG release: 14.3 % (pH 7.4; 20 h) 19.5% (pH 7.4; 72 h) 27.1% (pH 5.2; 20 h) 35.2% (pH 5.2; 72 h)	covalent bond formation between ICG (I) and WS_2-PEG 3) WID formation trough non-covalent bond formation between WI and DOX (D) 4) WID-M formation trough physical extrusion of WID and erythrocyte vesicles 5) WID-M-FA formation trough DSPE- PEG_{2000}-FA adsorption on WID-M membrane	Zeta potential: WS_2 = -16.5 mV WS_2-PEG = -7.4 mV DOX = -2.8 mV ICG = -5.5 mV M = -9.6 mV WID = -14.2 mV WID-M = -24.9 mV WID-M-FA = -30.9 mV	
N-WS_2	-	N-WS_2 formation by hydrothermal reaction	Improved stability in water and biocompatibility Improved absorption in the NIR region	[38]
WS_2-IO-MS-PEG/DOX	DOX Drug loading: 13.5% (WS_2-IO-MS-PEG: DOX weight ratio: n/s, pH 8) Drug release: 10.6 % (pH 7.4; 5 h) 12.5% (pH 7.4; 24 h)	1) Covalent bond formation between DMSA-modified IONPs and WS_2 2) Covalent bond formation between SiO_2 and WS_2-IO 3) PEG adsorption on WS_2-IO-MS surface	Improved stability in water, saline and serum	[32]

 doi:10.20944/preprints202410.1155.v1

	11.9% (pH 5.5; 5 h) 42.5% (pH 5.5; 24 h)	4) DOX adsorption on WS_2-IO-MS-PEG		
PEG-WS_2:Gd^{3+}	-	1) Covalent bond formation between WS_2 and Gd^{3+} 2) C_{18}PMH-PEG adsorption on WS_2:Gd^{3+} surface	Improved stability in water, saline, PBS, 1640-Medium and FBS	[39]
WS_2 -lipid	DOX Drug loading: 87% (WS_2 -lipid: DOX weight ratio 1:5, pH 7.4) Drug release: 13.3% (pH 7.4; 8 h) 32.1% (pH 7.4; 168 h) 22.3% (pH 5; 8 h) 43.2% (pH 5;168 h)	1) Liposomes formation by membrane hydration methods 2) WS_2 -lipid formation by liposomes adsorption on WS_2 surface 3) DOX adsorption on WS_2 -lipid	Improved stability in distilled water, PBS and RPMI-1640 medium containing 10% fetal bovine serum Zeta potential: WS_2 = -42.9 mV Liposome = -25.87 mV WS_2 -lipid = -33.77 mV	[35]
mWS_2-lipid	DOX Drug loading: 179.53% (WS_2 -lipid: DOX weight ratio 1:2) Drug release: 12.5% (pH 7.4; 8 h) 33% (pH 7.4; 168 h) 23% (pH 5; 8 h) 48% (pH 5;168 h)	1) mWS_2 formation by solvothermal reaction 2) Liposome adsorption on mWS_2 3) DOX adsorption on mWS_2-lipid	Improved stability in water, PBS and DMEM Zeta potential: WS_2 = −42.96 mV mWS_2 = −46.25 mV mWS_2-lipid = −24.74 mV Lipid = -24.66 mV Superparamagnetic properties	[36]

 doi:10.20944/preprints202410.1155.v1

WS_2/Au-lipid-DOX	DOX Drug loading: 84.54% (WS_2/Au-lipid: DOX weight ratio n/s, pH 7.4) Drug release: 12.5% (pH 7.4; 8 h) 24% (pH 7.4; 168 h) 17% (pH 5; 8 h) 42.5% (pH 5; 168 h)	1) WS_2/Au was synthesized using $Na_3C_6H_5O_7$ reduction method 2) WS_2/Au-lipid by magnetic stirring 3) DOX adsorption on WS_2/Au-lipid	Improved stability in water, PBS and DMEM Zeta potential: WS_2 = −42.19 mV WS_2/Au = −40.61 mV WS_2/Au-lipid = −44.72 mV Lipid = -36.79 mV	[37]

3. Drug Loading and Release

The large surface area of WS_2-based materials makes them great platforms for drug delivery and PTT. Their surface can be modified not only to improve biocompatibility and water stability but also to facilitate and improve drug loading. Physical adsorption is a common approach, where the drugs are adsorbed through non-covalent interactions, such as hydrogen bonds or van der Waals forces. Drugs can also be conjugated via covalent bonding, involving functional groups at the 2DnMat surface [41]. Drug release is usually triggered by changes in temperature, pH or light exposure. This allows the release on the target site, enhancing the therapy efficacy and minimizing the size effects [41]. PTT involve the use of NIR light, which triggers drug release by temperature increase. The pH mediated target release is also a commonly used strategy. Usually, the tumor exhibits an acidic pH and so the drug carriers can be adapted in order to release in acidic environment [41].

The combination of WS_2 nanoparticles and drugs, such as DOX, has been studied to optimize loading and release optimum conditions. Fe(III)-WS_2-PVP nanocapsules have high DOX loading capacity and, because of the continuous redox reactions between Fe(III) and WS_2, Fe^{2+} triggers the biodegradation of the Fe(III)-WS_2 -PVP nanocapsules and consequent release of DOX. The optimal drug loading capacity of these nanocapsules was found to be 41 %, with concentrations of Fe(III)-WS_2-PVP and DOX of 500 μg mL^{-1}. The drug release profiles demonstrated the pH dependence and the increase in the efficacy of the Fe(III)-WS_2 -PVP in comparison to WS_2 -PVP. After 48 h, the drug release was 12.7 % at pH 7.4 and 48.2 % at pH 6 [34]. Long et al. [40] investigated the possibility of using membrane systems for surface modifications to improve the drug delivery and photothermal capacity of the NPs (**Figure 1a**). WID-M-FA was produced first by the adsorption of DOX and ICG at WS_2-PEG surface and then by the coating with DSPE-PEG_{2000}-FA-modified erythrocyte membrane. These nanoparticles have a drug loading of 22.9% and 24.2% for ICG and DOX, respectively. After 72 h, at pH 7.4, 30.9% DOX and 19.5% ICG were released from the WID-M-FA, which represents a decrease compared to the release of the WID without coating (44.3% DOX and 35.2% ICG). For a pH of 5.8, 70.9% DOX and 38.6% ICG were released from the WID NPs, and 56.4% DOX and 35.2% ICG after the coating with the erythrocyte membrane (**Figure 1b**). These results suggest that the erythrocyte membrane reduces the drug release, improving the accumulation of the drug at the tumor site. With NIR irradiation (808 nm laser, 1 W cm^{-2}) for 30 min, the release of DOX was 30% at pH 5.2, 3 times higher than that of the control.

 doi:10.20944/preprints202410.1155.v1

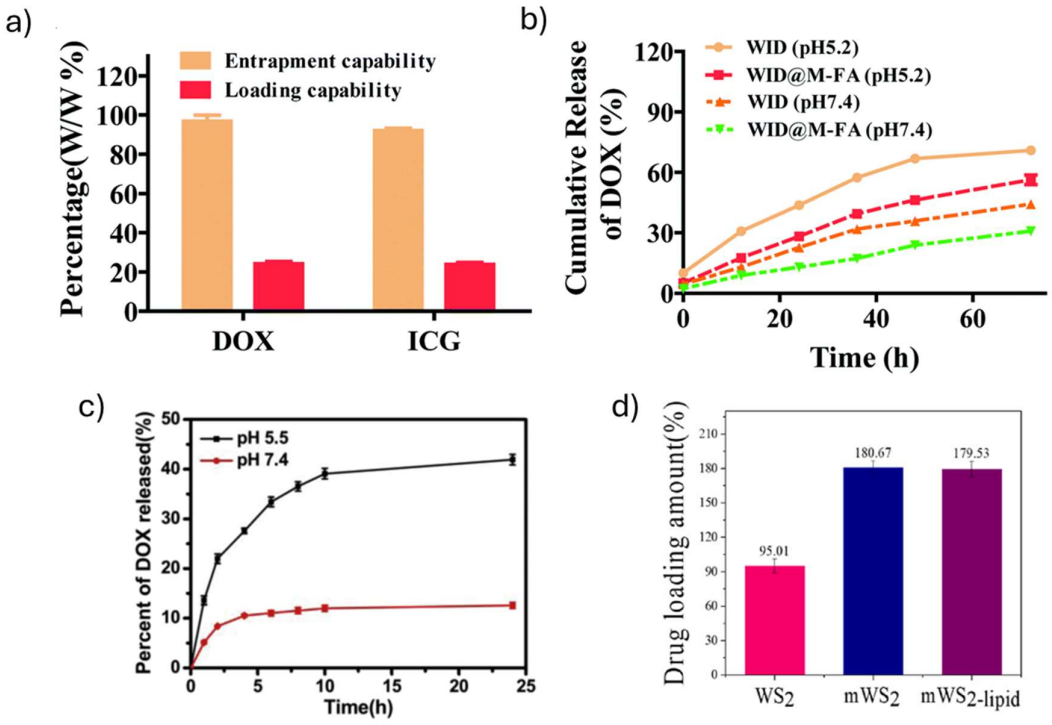

Figure 1. Drug loading and release of WS_2 nanoparticles. Top: a) DOX and ICG loading and entrapment efficiency of WID NPs with the WS_2, DOX and ICG concentrations of 1 mg mL $^{-1}$, 0.5 mg mL^{-1}, and 0.5 mg mL $^{-1}$, respectively. b) DOX release behavior of WID and WID@M-FA NPs at pH 7.4 and 5.2. (a) and (b) adapted with permission.[40] © The Royal Society of Chemistry 2020; Bottom: c) DOX release from WS_2-IO@MS-PEG/DOX NPs overtime at different pH values (5.5 and 7.4). Adapted with permission.[32] Copyright © 2015 Elsevier Ltd. d) The drug loading of WS_2, mWS_2 and mWS_2-lipid. Adapted with permission. [36] © 2023 Elsevier B.V. All rights reserved. Abbreviations: DOX, doxorubicin; ICG, indocyane green; mWS_2, WS_2 loaded with iron oxide nanoparticles; WID, WS_2 loaded with DOX and ICG; WID-M-FA, WS_2 loaded with DOX and ICG, and modified with an erythrocyte membrane.

The loading of DOX at the surface of WS_2-IO-MS-PEG/DOX reached a maximum of 13.5% for 0.5 mg mL^{-1} concentration. The drug release showed pH dependence, being the acidic medium the most favorable, with 42.5% release at pH 5.5 after 24h, versus 12.5% at pH 7.4 **(Figure 1c)**. A NIR-triggered DOX release was also tested in PBS at pH 5.5 and 7.4, with 808 nm laser irradiation (5 min, 0.8 W cm^{-2}). For pH 5.5, a release of 43 % was reached, while at pH 7.4, a released of about 25% was obtained at the same time point [32]. In a different study, the DOX loading rate at the surface of WS_2 was 95 %, while for WS_2-lipid, WS_2 coated with liposomes by electrostatic adsorption it decreased to 87 %, at pH 7.4. The biggest difference was found regarding the stability of both dispersions. While WS_2-DOX showed strong aggregation, WS_2-lipid-DOX was well dispersed under physiological conditions. DOX cumulative release from WS_2-lipid nanoparticles, after 168 h, at pH 7.4 was of 32.1%, while at pH 5 it was of 43.2% [35]. DOX was also conjugated with lipid-modified WS_2 loaded with a magnetic nanoparticle (m-WS_2), iron oxide, by a solvothermal method. The IONPs have high targeting ability, due to their magnetic targeting properties, which can be used for targeted release of the drug at the tumor site. The drug loading was about 95% for WS_2 alone. After magnetization, drug loading increased about 2 times to 180% (**Figure 1d**). After lipid modification, drug loading stayed the same. This indicates that the liposomes did not affect the loading of DOX, which was also proved by fluorescence scanning, which suggests that the DOX was loaded on the m-WS_2 surface and, therefore, wasn't adsorbed onto the lipids. The drug release curves suggest a pH dependence. After 168 h, about 24% of DOX was released at pH 7.4 and 42.5% at pH 5, for the m-WS_2-lipid NPs. Also,

 doi:10.20944/preprints202410.1155.v1

the m-WS_2-lipid-DOX and m-WS_2-DOX release curves were similar, suggesting that the lipid modification didn't influence the drug release [36]. DOX was also loaded in WS_2/Au-lipid nanoparticles. WS_2/Au was produced using the sodium citrate reduction method, where WS_2 is magnetically stirred for 30 min with a solution of sodium citrate ($C_6H_5Na_3O_7$) and chloroauric acid ($HAuCl_4$). Then, liposomes were produced through thin film dispersion and were mixed with the previous solution, resulting in WS_2/Au-lipid nanoparticles. Their loading with DOX was tested and reached a loading rate of about 85%, slightly worse than WS_2 and WS_2/Au, which was about 90%, similar to WS_2-lipid, which is about 2 times worse than m-WS_2-lipid [35,36]. The difference resides in the stability that the lipid modification provides, having better stability than the other conjugates. Drug release was about 20% higher in an acidic environment (pH 5.0) than in a neutral one (pH 7.4). At pH 5.0, DOX release from WS_2/Au was 48%, while DOX release from WS_2/Au-lipid was 42%. This indicates that the lipid modification decreased the DOX release [37].

4. In Vitro Biocompatibility Studies

A biocompatible nanomaterial should be able to interact with cells or organisms without causing them harm [42]. Therefore, it is important to determine parameters such as material size, structural morphology, hydrophilicity, dispersibility in water, surface chemistry, and concentration, which are directly related to their biocompatibility. In order to access materials' biocompatibility, in vitro and in vivo studies should be performed before their use in biomedicine [8].

WS_2 biocompatibility has been explored in several studies. **Table 2** compiles current literature on WS_2-based materials tests with cell lines and the impact of the different materials on cell viability and particle internalization, among others.

Table 2. *In vitro* biocompatibility studies for tungsten disulfide-based materials.

2D material	Particle size (nm)	Culture conditions and cell viability	2DnMat location	Additional outcomes	Reference
WS_2 – BSA	150-200	WS_2 –BSA (HeLa1, 2, 24, 36, 48 h incubation) >80% (6.25 ppm) >70% (12.5 ppm) >70% (25 ppm) >80% (50 ppm) Concentrations tested: 6.25-50 ppm	-	-	[33]
Fe (III)- WS_2 -PVP	108	Fe (III)- WS_2 -PVP (HT29, 24 h incubation) > 80% (100 μg mL^{-1})	-	-	[34]

 doi:10.20944/preprints202410.1155.v1

WS_2 – PEG	94	WS_2 – PEG (4T1, 24 h incubation) > 90% (0.1 mg mL^{-1}) WS_2 – PEG (HeLa, 24 h incubation) > 90% (0.1 mg mL^{-1}) WS_2 – PEG (293T, 24 h incubation) > 90% (0.1 mg mL^{-1}) Concentrations tested: 0.006-0.1 mg mL^{-1}	-	LDH release (4T1, HeLa, 293T, 24 h incubation): 0% (100 μg mL^{-1}) ROS generation (4T1, HeLa, 293T, 24 h incubation): 7% (50, 100 μg mL^{-1}) Concentrations tested: 13–100 μg mL^{-1}	[28]
WS_2-IO-MS-PEG/DOX	90	WS_2-IO-MS-PEG/DOX (4T1, 24 h incubation) > 70% (0.781 μg mL^{-1}) > 60% (1.563 μg mL^{-1}) > 60% (3.125 μg mL^{-1}) > 60% (6.25 μg mL^{-1}) > 30% (12.5 μg mL^{-1}) > 20% (25 μg mL^{-1}) Concentrations tested:0.781-0.25 μg mL^{-1}	-	-	[32]
WID-M-FA	162	WI-M-FA (HeLa, 24 h incubation) 89% (12.5 μg mL^{-1}) 89% (25 μg mL^{-1}) 75.9% (50 μg mL^{-1}) 68.5% (100 μg mL^{-1})	Observed in lysosomes (4 h incubation)	1% hemolysis (100 μg mL^{-1}, 4 h incubation with RBCs)	[40]

 doi:10.20944/preprints202410.1155.v1

		Concentrations tested: 12.5-100 μg mL^{-1}			
N- WS_2	150	N- WS_2 (Hela, 24 h incubation) >90% (15 μg mL^{-1}) >88% (120 μg mL^{-1}) N- WS_2 (MDA-MB-231, 24 h incubation) >90% (15 μg mL^{-1}) >90% (120 μg mL^{-1}) N- WS_2 (HepG2, 24 h incubation) >90% (15 μg mL^{-1}) >90% (120 μg mL^{-1}) Concentrations tested: 0.469-120 μg mL^{-1}	-	-	[38]
PEG-WS_2:Gd^{3+}	90-100	PEG-WS_2:Gd^{3+} (4T1, 24, 48 h incubation) >90% (50 μg mL^{-1}) Concentrations tested: 1.56-100 μg mL^{-1}	-	-	[39]
WS_2 -lipid-DOX	222.58	WS_2 -lipid (MCF-7, 24 h incubation) > 90% (100 μg mL^{-1}) Concentrations tested: 2.5-200 μg mL^{-1} WS_2 -lipid-DOX (MCF-7, 24 h incubation) > 80% (1, 2.5, 5 μg mL^{-1})	Observed in cytoplasm (MCF-7, 4 h incubation)	-	[35]

 doi:10.20944/preprints202410.1155.v1

		> 40% (12. 5 μg mL^{-1}) > 30% (25 μg mL^{-1}) > 20% (50 μg mL^{-1}) Concentrations tested: 1-50 μg mL^{-1}			
mWS_2-lipid	318.07	mWS_2-lipid (MCF-7, 4 h incubation) >90% Concentrations tested: 1-50 μg mL^{-1} mWS_2-lipid-DOX (MCF-7, 4 h incubation) 50% (2.5 μg mL^{-1}) 34% (5 μg mL^{-1}) 22% (12.5 μg mL^{-1}) 17% (25 μg mL^{-1}) 14% (50 μg mL^{-1}) Concentrations tested: 2.5-50 μg mL^{-1}	Observed in cytoplasm (MCF-7, 24 h incubation)	-	[36]
WS_2/Au-lipid-DOX	196	WS_2/Au-lipid (MCF-7, 4 h incubation) >90% (50 μg mL^{-1}) Concentrations tested: 2-50 μg mL^{-1} WS_2/Au-lipid-DOX (MCF-7, 4 h incubation) >68% (2.5 μg mL^{-1}) >50% (5, 12.5 μg mL^{-1}) >41% (25 μg mL^{-1}) >33% (50 μg mL^{-1})	Observed in cytoplasm (MCF-7, 4 h incubation)	-	[37]

 doi:10.20944/preprints202410.1155.v1

	Concentrations tested: 2.5-50 μg mL^{-1}

BSA, bovine serum albumin; DOX, doxorubicin; IO, iron oxide; LDH, lactate dehydrogenase; MS, mesoporous; PEG, polyethylene glycol; PVP, poly(vinylpyrrolidone); RBCs, red blood cells; ROS, reactive oxygen species.

WS_2-BSA nanosheets were tested for cytotoxicity following the MTT assay with HeLa cells, with incubation times of 2, 24, 36, and 48 h. The overall cell viability was found to be always above 70% for concentrations between 6.25 ppm and 50 ppm. For a concentration of 50 ppm, the cell survival was above 80% [33]. The cytotoxicity of WS_2-PEG was also evaluated through this assay, using 4T1, HeLa, and 239T cells. After 24 h, no signs of toxicity were observed, even for concentrations as high as 0.1 mg mL^{-1}, with cell viability remaining higher than 90 %. A lactate dehydrogenase (LDH) study was also made to examine any potential damage to the cells caused by WS_2-PEG, results showed that the level of LDH release was normal, indicating that the nanoparticles caused no damage to the cells [28].

WI NPs were produced by mixing WS_2-PEG and Indocyanine green (ICG). From WI NPs, WI-M-FA NPs were produced by the sonication of an erythrocyte vesicle (M) with WI NPs, resulting in WI-M NPs. Finally, the addition of DSPE-PEG_{2000}-FA to this dispersion yielded WI-M-FA NPs. Through the MTT assay, the cytotoxicity of these NPs was studied with concentrations ranging from 12.5 to 100 μg mL^{-1} incubated with HeLa cells for 24h. The cell viability after incubation with WI-M-FA for 24h was above 90%, for all concentrations, in contrast to WI, which killed the cells in a concentration-dependent manner. The cell viability of these NPs decreased with the increase in concentrations, from 89% (12.5 μg mL^{-1}) to 68.5% (100 μg mL^{-1}) [40]. The uptake by the macrophages, was also studied by incubating RAW264.7 macrophages with WID-M-FA and WID NPs. Through the CLSM images, it is possible to observe that the intracellular fluorescence signal of the WID NPs increased by more 70% compared to the WID-M-FA NPs signal, which indicates that the addition of the erythrocyte membrane reduced the uptake of the NPs by the macrophages, which can improve the uptake of the nanocarrier in the tumor, by prolonging the blood circulation time of the NPs. A live/dead staining revealed that the combination of WID-M-FA with NIR laser irradiation (808 nm, 1 W cm^{-2}, 5 min) killed more than 70% of the tumor cells (**Figure 2a**) [40].

 doi:10.20944/preprints202410.1155.v1

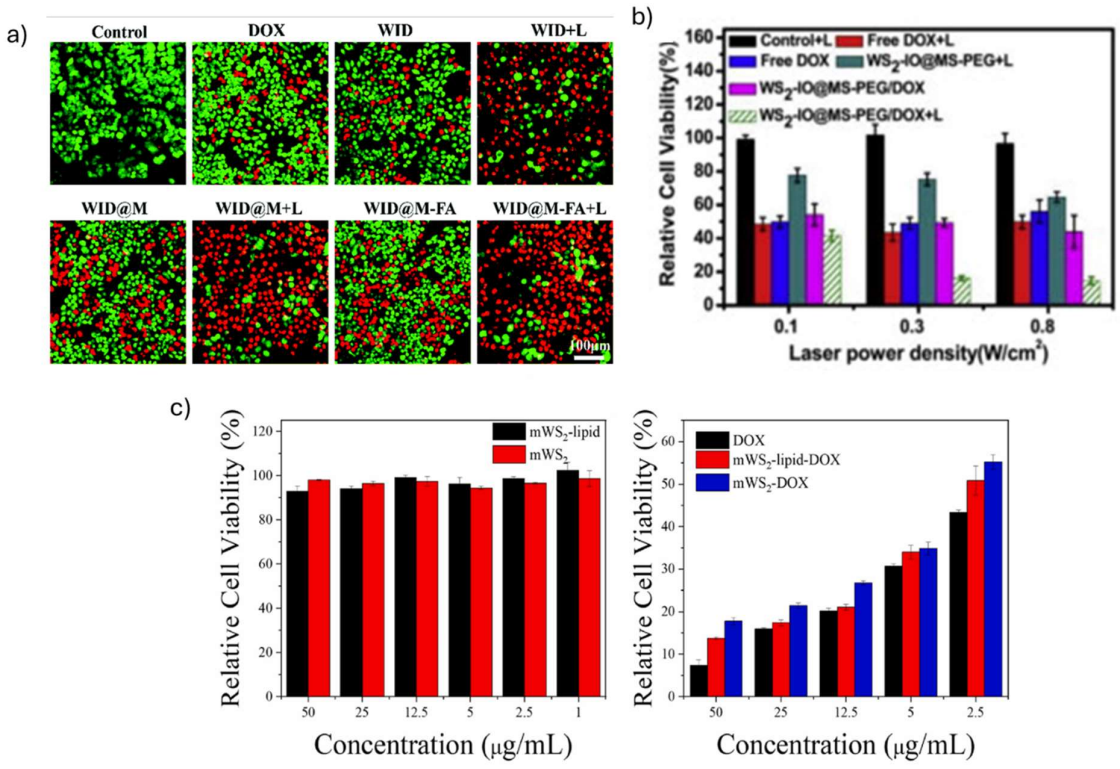

Figure 2. In vitro cytotoxicity of WS_2 nanomaterials. (a) Live/dead staining of HeLa cells cultured with different formulations with or without 808 nm NIR laser irradiation (1 W cm^{-2}, 5 min) of WID@M-FA NPs. Adapted with permission.[40] © The Royal Society of Chemistry 2020; (b) Relative viabilities of 4T1 cells after various treatments with WS_2-IO@MS-PEG/DOX. Adapted with permission.[32] Copyright © 2015 Elsevier Ltd. (c) Relative viability of mWS_2 and mWS_2-lipid co-incubated with MCF-7 for 24 h and of free DOX, mWS_2-DOX and mWS_2-lipid-DOX. Adapted with permission. [36] © 2023 Elsevier B.V. All rights reserved. Abbreviations: DOX, doxorubicin; ICG, indocyane green; mWS_2, WS_2 loaded with iron oxide nanoparticles; PEG, polyethylene glycol; WID, WS_2 loaded with DOX and ICG; WID-M-FA, WS_2 loaded with DOX and ICG, and modified with an erythrocyte membrane; WS_2-IO-MS-PEG-DOX, WS_2 functionalized with iron oxide nanoparticles, coated with mesoporous silica and functionalized with PEG.

WS_2 nanosheets functionalized with iron oxide nanoparticles, coated with mesoporous silica, and then functionalized with polyethylene glycol (PEG), WS_2-IO-MS-PEG, were produced to improve the drug loading and release capacity of WS_2, for cancer therapy applications. According to the MTT assay, these nanomaterials showed no sign of toxicity towards different types of cells, namely 4T1 murine breast cancer cells, HeLa human cervical cancer cells, and 293T human embryonic kidney cells, even for concentrations as high as 200 μg mL^{-1} (**Figure 2b**). The conjugation of WS_2-IO-MS-PEG and DOX was also tested for impact on cell viability. For a concentration of 25 μg mL^{-1}, the viability of 4T1 cells, was of 20% after 24 h [32]. WS_2/Au-lipid, gold-doped WS_2 nanosheets modified with lipids, showed no toxicity when incubated with MCF-7 cells, after 4 h cell viabilities above 90% were obtained. The same test was made for WS_2-lipid and m-WS_2-lipid (**Figure 2c**), with similar results being obtained. However, after DOX loading, the conjugate (WS_2/Au-lipid-DOX) decreased cell viability up to a minimum of 33%, at a concentration of 50 μg mL^{-1} [37]. The drug-loaded complex of WS_2-lipid-DOX and m-WS_2-lipid-DOX also caused concentration-dependent cell viability decreases, reaching even lower cell viability values of 20% and 14%, respectively (50 μg mL^{-1}) [35–37].

Human colorectal carcinoma (HT29) cells were incubated for 24 h with Fe(III)-derived WS_2 nanosheet coated with PVP, Fe(III)-WS_2-PVP nanocapsules (100 μg mL^{-1}), resulting in a cell viability

 doi:10.20944/preprints202410.1155.v1

of 85.6 %. Furthermore, the potential influence of the degradation products in cell viability was also studied. Fe(III)@WS_2-PVP nanocapsules were degraded in PBS for 7 days, and the viability of HT29 cells was not influenced (98.3%) [34].

For N-WS_2, an ammonia-intercalated WS_2 ultrathin nanosheet, the cell viability was higher than 90%, after 24 h of incubation with HeLa cells, MDA-MB-231 cells, and HepG2 cells, at concentrations up to 120 μg mL^{-1}. Also, there was no sign of cell proliferation decrease [38].

The cytotoxicity of PEG-WS_2:Gd^{3+} was also studied based on the MTT assay in 4T1 murine breast cancer cells incubated with different concentrations for 24 h and 48h. It was observed that cell viability was above 90%, for concentrations as high as 50 μg mL^{-1} [39].

Most WS_2-based nanoparticles had cell viability in the range of 80-90 %, which is above the limit toxicity reported in ISO10993-5:2009(E) [43]. These NPs did not show a concentration-dependent viability, except for WI-M-FA, which showed a decrease in cell viability as the concentration increased. Regarding nanoparticle-drug conjugates, cell viability follows a clear concentration dependence. The cell viability of MCF-7 incubated with m-WS_2-lipid-DOX decreased from 50% to 15%, when increasing concentrations from 2.5 μg mL^{-1} to 50 μg mL^{-1}. When the cells were incubated with WS_2-Lipid DOX, the cell viability decreased from 100% to 20%, with concentrations of 1 μg mL^{-1} and 50 μg mL^{-1}. WS_2-IO-MS-PEG/DOX reached a 20 % viability for only 25 μg mL^{-1}, while WS_2-lipid, m-WS_2-lipid and WS_2/Au/lipid reached 30%, 17% and 41%, respectively, at the same concentration.

5. In Vivo Biocompatibility Studies

Biological models are often used to test the biocompatibility of new nanomaterials. **Table 3** presents current studies on tungsten disulfide-based materials in vivo biocompatibility.

Table 3. *In vivo* biocompatibility studies for tungsten disulfide-based materials.

2D material	Animal model	Animal survival	Treatment Conditions	Main Results	Reference
WS_2 – BSA	Zebrafish embryos	120 h: >80%	Zebrafish embryos were incubated in E3 medium with WS_2 – BSA Concentrations tested: 0-50 ppm	120 h: Hatching rate: 50% (0 ppm) 27.5% (6.25 ppm) 32.5% (12.5 ppm) 45% (25 ppm) 48.5% (50 ppm)	[33]
Fe (III)-WS_2 -PVP	HT29 colorectal carcinoma bearing KM mice	-	i.v. administration (100 μg mL−1) Heart: 1 day: 0,03 μg g^{-1} 7 days: 0,11 μg g^{-1} Liver: 1 day: 0,52 μg g^{-1} 7 days: 0,25 μg g^{-1} Spleen: 1 day: 0,77 μg g^{-1} 7 days: 0,18 μg g^{-1} Lung: 1 day: 0,22 μg g^{-1} 7 days: 0,07 μg g^{-1}	28 days: no changes on heart, liver, spleen, lung and kidney tissues	[34]

 doi:10.20944/preprints202410.1155.v1

			Kidney: 1 day: 0,07 μg g^{-1} 7 days: 0,02 μg g^{-1}		
WS_2 – PEG	4T1 tumor bearing Balb/C mice	-	i.t administration (2 mg kg^{-1}, 30 min) i.v. administration (20 mg kg^{-1}, 24 h) No changes on body weight 28 days: serum biochemistry markers on normal variation ranges (ALT, ALP, AST, BUN levels, WBC, RBC, HCT, Hgb, MCV, MCH, MCHC, and platelets)	45 days: no changes on liver, spleen, kidney, heart and lung	[28]
WS_2-IO-MS-PEG/DOX	4T1 tumor bearing Balb/C mice	-	i.v. administration (WS_2 = 8.4 mg kg^{-1}, DOX = 7 mg kg^{-1}, 24 h) Circulation half-life = 4.77 h Heart: 24 h: 1.18% ID g^{-1} Liver: 24 h: 25.88% ID g^{-1} Spleen: 24 h: 38.82% ID g^{-1} Lung: 24 h: 5.29% ID g^{-1} Kidney: 24 h: 4.71% ID g^{-1} Stomach: 24 h: 2.35% ID g^{-1} Intestine: 24 h: 1.76% ID g^{-1} Muscle: 24 h: 1.76% ID g^{-1} Tumor: 24 h: 8.24% ID g^{-1}	24 h: high accumulation on liver spleen and tumor	[32]

 doi:10.20944/preprints202410.1155.v1

WID-M-FA	HeLA tumor-bearing Balb/c mice	-	i.v. administration (DOX = 2 mg kg^{-1}, ICG = 5 mg kg^{-1}, 24 h) 18 days: serum biochemistry markers on normal variation ranges (RBC, RDW, MCHC, MCV, PLT, WBC, ALT, AST, CRE, BUN)	18 days: no changes on liver, spleen, kidney, heart and lung	[40]
N- WS_2	HeLa tumor-bearing female NOD/SCID mice	-	i.t administration (1.2 mg mL^{-1}, 40 μL, 24 h) 16 days: serum biochemistry markers on normal variation ranges (WBC, RBC, Hb, HCT, PLT, MCV, MCHC, MCH)	48 h: no changes in liver and lung tissues	[38]
PEG-WS_2:Gd^{3+}	4T1 tumor-bearing Balb/c mice	-	i.v. administration (2 mg mL^{-1}, 200 μL, 24 h) Tumor: 24h: 11.8% ID g^{-1} Liver: 24 h: 50.9% ID g^{-1} Spleen: 24 h: 94.5% ID g^{-1}	T1-MR signal (a.u.): 200 (before i.v. injection) 500 (after i.v. injection)	[39]

ALP, Alkaline phosphatase; ALT, Alanine aminotransferase; AST, Aspartate aminotransferase; BSA, bovine serum albumin; BUN, blood urea nitrogen; CRE, creatinine; DOX, doxorubicin; HCT, hematocrit; Hgb, hemoglobin; ICG, Indocyanine green; ID, injected dose; IO, iron oxide; i.t., intratumoral; i.v., intravenous; KM, Kunming mouse; MCH, mean corpuscular hemoglobin; MCHC, mean corpuscular hemoglobin concentration; MCV, Mean corpuscular volume; MS, mesoporous; NOD/SCID, nonobese diabetic/severe combined immunodeficiency; PEG, polyethylene glycol; PLT, platelet; PVP, poly(vinylpyrrolidone); RBC, red blood cells; RDW, red blood cell distribution width; WBC, white blood cells.

Zebrafish embryos were used to study the influence of WS_2–BSA nanosheets on the survival rate of the fertilized embryos. The survival rate for different concentrations was found to be above 80% for incubation times as high as 120 h and followed the same trend as the control group. This indicates that the WS_2–BSA nanosheets presented low toxicity. With time, the embryos started to hatch, and the hatching rate was affected by increasing concentrations of WS_2-BSA NPs with which they were incubated. WS_2-BSA NPs delayed the hatching time of the embryo groups in the two first incubation stages, 72 h and 96h. After 120 h, the incubation rate of the embryos incubated with WS_2-BSA started to catch up with the control group, suggesting that the delay in hatching caused by the NPs was overcome with time, especially for high concentrations [33].

Fe(III)-WS_2-PVP was intravenously administrated to HT29 colorectal carcinoma-bearing KM mice, and their biodegradation profile was studied by inductively coupled plasma atomic emission

 doi:10.20944/preprints202410.1155.v1

spectroscopy (ICP-AES). It was found that there was an accumulation of the W element in the liver and spleen, organs responsible for the excretion of particles from the blood, on the first day, which ends up decreasing over the cross of 28 days (**Figure 3a**). The overall distribution of W in the organs was very low after 7 days of the administration. From the hematoxylin and eosin (H&E) staining tests, there was no sign of changes on the major organs during the 28 days due to the fast in vivo biodegradation, proving the good biocompatibility of these nanomaterials (**Figure 3b**) [34]. For WID-M-FA NPs, a dose of 2 mg kg^{-1} DOX and 5 mg kg^{-1} ICG was administered intravenously to HeLa tumor-bearing Balb/c mice. After 24 h, results revealed that the nanoparticles did not affect the blood parameters tested (**Table 3**), in contrast with what occurred with just DOX administration. These results suggest that the modifications reduce DOX leakage in the blood circulation. Furthermore, the side effects of the WID@M-FA NPs on the liver and kidney were studied. Histological analysis of kidney, lung, spleen, liver and heart showed no effect of the NPs on renal and hepatic functions, in contrast with the DOX control injection, that induced hepatotoxicity and nephrotoxicity [40]. HeLa tumor-bearing female NOD/SCID mice intratumorously administered with 1.2 mg mL^{-1} N-WS_2, also displayed normal blood parameters (**Figure 3c**) [38].

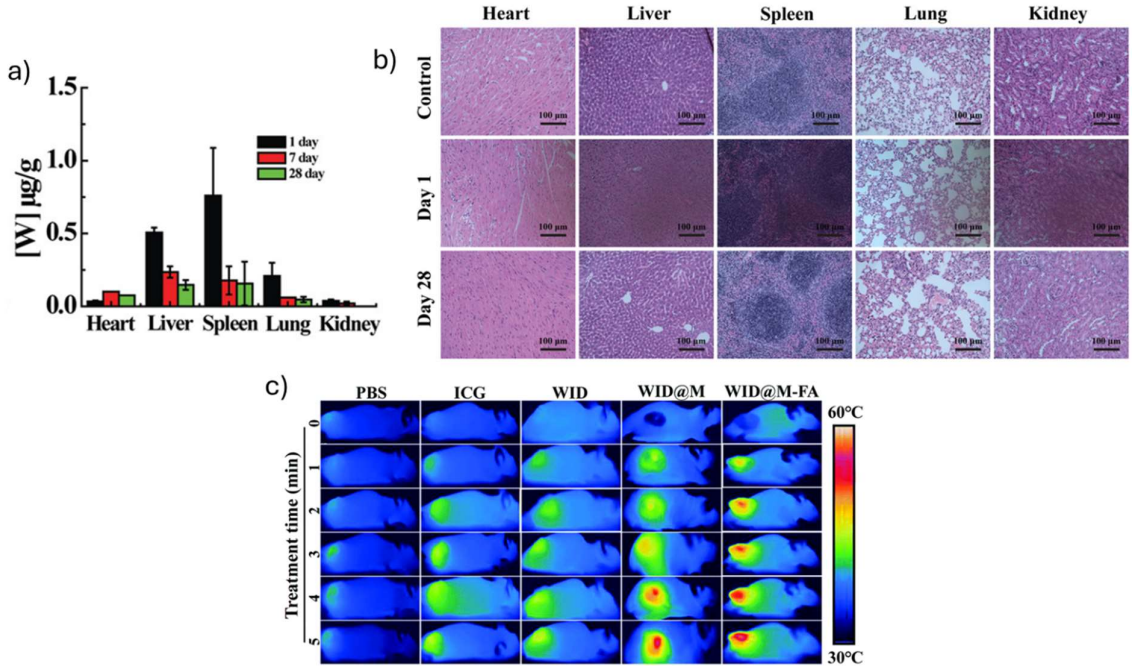

Figure 3. *In vivo* biocompatibility studies for WS_2-based nanomaterials. (a) W biodistribution of mice injected with Fe(III)@WS_2-PVP nanocapsules. (b) H&E-stained tissue sections of major organs of KM mice that received saline or Fe(III)@WS_2-PVP nanocapsules injection. (a) and (b) adapted with permission. [34] © 2019 WILEY-VCH Verlag GmbH & Co. KGaA, Weinheim. (c) Infrared thermal images and heat map quantitative analysis of HeLa tumor-bearing mice after administering intravenous injection of PBS, ICG, WID, WID@M and WID@M-FA NPs and under 808 nm NIR laser irradiation (1 W cm^{-2}, 5 min). Adapted with permission. [40] © The Royal Society of Chemistry 2020. Abbreviations: DOX, doxorubicin; Fe(III)@WS_2-PVP, WS_2 conjugated with Fe(III) and modified with PVP ; ICG, indocyane green; PVP, Poly(vinylpyrrolidone); WID, WS_2 loaded with DOX and ICG; WID-M-FA, WS_2 loaded with DOX and ICG, and modified with an erythrocyte membrane.

To evaluate the WS_2-PEG toxicological profile, a serum biochemistry assay and complete blood tests were performed on Balb/C mice intravenously injected (2 mg kg^{-1}) or intratumorously injected (2 mg kg^{-1}) with WS_2-PEG, after 1, 14, and 28 days. All parameters were within standard limits, with WS_2-PEG NPs causing no toxicity to the animals [28]. Similar studies were conducted with WS_2-IO-MS-PEG/DOX, WS_2 nanosheet functionalized with iron oxide, coated with mesoporous silica, and functionalized with PEG. Doses of 8.4 mg kg^{-1} WS_2 and 7 mg kg^{-1} DOX were intravenously injected

 doi:10.20944/preprints202410.1155.v1

into tumor-bearing Balb/C mice. After 24 h, inductively-coupled plasma atomic emission spectroscopy (ICO-AES) results showed high retention in the liver and spleen. Apart from this, a relativity high amount of W was found in the tumor after 24 h. This high tumor retention is directly related to the long blood circulation half-life, 4.77 h, which enhances the permeation and retention of the nanomaterials in the tumors. The tumor uptake was 8.24% of the injected dose per gram of tissue (% ID/g) [32]. The same trend can be seen in the analysis of PEG-WS_2:Gd^{3+}, where after intravenous administration of 2 mg mL^{-1} to 4T1 tumor-bearing Balb/c mice, high accumulation on the liver and spleen, followed by tumor concentration was found. In this case, the tumor uptake, measured by ICP, was 11.8% ID/g [39].

Several studies report histology results that show no signs of toxicity in the liver, spleen, kidney, heart and lungs after 48 h to 45 days of WS_2-based materials administration, even for doses as high as 20 mg kg^{-1}. However, other studies report a high accumulation of nanoparticles especially in the spleen, liver, and tumor. However, in all cases no toxicity has been found and tumor accumulation was identified.

6. In Vitro Photothermal Therapy Studies

Different variables must be considered when doing PTT studies, such as the light source type and features, time of irradiation, concentration of the photothermal agent, among others. **Table 4** congregates in vitro PTT studies using tungsten disulfide-based materials available.

Table 4. *In vitro* photothermal therapy studies using tungsten disulfide-based materials.

2D material	Irradiation method	Energy (W cm^{-2})	Time of irradiation (min)	Culture conditions and cell viability	Reference
WS_2 – BSA	Laser (808 nm)	1.5	5	T_{max} = 44.5 °C (1.5 W cm^{-2}, 5 min) WS_2 – BSA (HeLa, 24 h incubation) 65% (6.25, 12.5 ppm) 40% (25 ppm) 35% (50 ppm)	[33]
Fe (III)-WS_2-PVP	Laser (808 nm)	1	5	T_{max} = 46 °C (1 W cm^{-2}, 5 min) DOX-Fe (III)-WS_2-PVP (HT29, 24 h incubation) 5.2% (250 μg mL^{-1})	[34]
WS_2 – PEG	Laser (808 nm)	0.1, 0.3, 0.5, 0.8	5	WS_2 – PEG (4T1, 6 h incubation) 100% (0.1 W cm^{-2}, 0.1 mg mL^{-1}) 72.7% (0.3 W cm^{-2}, 0.1 mg mL^{-1}) 45.5% (0.5 W cm^{-2}, 0.1 mg mL^{-1}) 7.3% (0.8 W cm^{-2}, 0.1 mg mL^{-1})	[28]

 doi:10.20944/preprints202410.1155.v1

WS_2-IO-MS-PEG/DOX	Laser (808 nm)	0.1, 0.3, 0.8	20	WS_2-IO-MS-PEG/DOX (4T1, 24 h incubation) 41.3% (0.1 W cm^{-2}, 50 μg mL^{-1} DOX) 16% (0.3 W cm^{-2}, 50 μg mL^{-1} DOX) 14.7% (0.8 W cm^{-2}, 50 μg mL^{-1} DOX)	[32]
WID-M-FA	Laser (808 nm)	1	5	T_{max} = 60 °C (1 W cm^{-2}, 5 min) WID-M-FA (HeLa, 24 h incubation) 18.5% (1 μg mL^{-1} DOX and 10 μg mL^{-1} ICG)	[40]
N- WS_2	Laser (808 nm)	0.3, 0.45, 0.6, 0.75	10	T_{max} = 50 °C (0.6 W cm^{-2}, 4 min) N- WS_2 (HeLa, 6 h incubation) 89.4% (0.3 W cm^{-2}, 120 μg mL^{-1}) 71.2% (0.45 W cm^{-2}, 120 μg mL^{-1}) 40.4% (0.6 W cm^{-2}, 120 μg mL^{-1}) 30.8% (0.75 W cm^{-2}, 120 μg mL^{-1}) Concentrations tested: 15-120 μg mL^{-1}	[38]
PEG-WS_2:Gd^{3+}	Laser (808 nm)	0.8	5	PEG-WS_2:Gd^{3+} (4T1,12 h incubation) 75.5% (6.25 μg mL^{-1}) 51.1% (12.5 μg mL^{-1}) 28.9% (25 μg mL^{-1}) 4.4% (50 μg mL^{-1})	[39]
WS_2 -lipid	Laser (808 nm)	2	10	T_{max} = 60 °C (2 W cm^{-2}, 10 min) WS_2 -lipid (MCF-7, 24 h incubation). 78% (25 μg mL^{-1}) 43% (50 μg mL^{-1}) 18 % (100 μg mL^{-1}) 9% (200 μg mL^{-1})	[35]

 doi:10.20944/preprints202410.1155.v1

				WS_2 -lipid-DOX (MCF-7, 24 h incubation) 20% (50 μg mL^{-1} DOX)	
mWS2-lipid	Laser (808 nm)	2	10	T_{max} = 68.1 °C (1.5 W cm^{-2}, 10 min) mWS2-lipid (MCF-7, 24 h incubation). 77% (12.5 μg mL^{-1}) 58% (25 μg mL^{-1}) 30% (50 μg mL^{-1}) 16% (100 μg mL^{-1}) mWS2-lipid-DOX (MCF-7, 24 h incubation) 27% (50 μg mL^{-1} DOX)	[36]
WS2/Au-lipid-DOX	Laser (808 nm)	2	10	T_{max} = 75 °C (1.5 W cm^{-2}, 10 min) WS2/Au-lipid (MCF-7, 24 h incubation). 54% (12.5 μg mL^{-1}) 29% (25 μg mL^{-1}) 18% (50 μg mL^{-1}) 7% (100 μg mL^{-1}) WS2/Au-lipid-DOX (MCF-7, 4 h incubation) 30% (12.5 μg mL^{-1} DOX)	[37]

BSA, bovine serum albumin; DOX, doxorubicin; IO, iron oxide; MS, mesoporous; PEG, polyethylene glycol; PVP, poly(vinylpyrrolidone).

WS_2-PEG (0.1 mg mL^{-1}) was incubated with 4T1 cells for 6 h, followed by irradiation with an 808 nm laser at irradiances of 0.1, 0.3, 0.5, 0.8 W cm^{-2}, for 5 min, resulting in cell viabilities of 100%, 72.7%, 45.5% and 7.3%, respectively [28]. WS_2-IO-MS-PEG/DOX (50 μg mL^{-1} DOX), under the same laser conditions and with a time of irradiation of 20 min, decreased 4T1 cell viability to 41.4% (0.8 W cm^{-2}), 16% (0.3 W cm^{-2}), and 14.7% (0.8 W cm^{-2}) [32]. N-WS_2 also caused a similar effect to HeLa cells, with cell viabilities of 89.4%, 71.2%, 40.4%, and 30.8% being obtained for irradiances of 0.3, 0.45, 0.6 and 0.75 W cm^{-2}. A N-WS_2 concentration of 120 μg mL^{-1} was used, and irradiation performed with an 808 nm laser for 10 min [38]. The temperature of the tumors incubated with N-WS_2 and irradiated with laser increased rapidly to 50 °C within 4 min, an increment of 21 °C, and remained at 50 °C for 6 min more. PEG-WS_2:Gd^{3+}, PEGylated-WS_2 doped with the metal gadolinium (Gd^{3+}), was incubated for 4 h with 4T1 cells at concentrations of 6.25, 12.5, 25 and 50 μg mL^{-1}. When irradiated with an 808 nm laser with a power of 0.8 W cm^{-2} for 5 min, the cell viabilities decreased with the increase of the concentration, being of 75.5%, 51.1%, 29.9% and 4.4%, respectively [39]. A similar trend happened for WS_2–BSA, incubated with HeLa cells with a gradient of concentration between 6.25-50 ppm, where cell viability decreased from 65% to 35%. Furthermore, photothermal tests (50 ppm, 1.5 W cm^{-2})

 doi:10.20944/preprints202410.1155.v1

revealed a temperature increase from 26 ˚C to 44.5 ˚C, within 5 min. These tests suggest that the materials have the potential to be used for cancer PTT [33].

Studies concerning the cell viability of HT29 cells incubated with Fe(III)-doped WS_2 modified with PVP and/or DOX, Fe(III)-WS_2-PVP and DOX-Fe(III)-WS_2-PVP for PTT treatment were conducted. The viability of HT29 cells treated with Fe(III)-WS_2-PVP (250 μg mL^{-1}) and DOX-Fe(III)-WS_2-PVP (150 μg mL^{-1} WS_2 and 100 μg mL^{-1} DOX) decreased to 37.7% and 5.2%, respectively, upon 808 nm laser irradiation (1 W cm^{-2}, 5 min). As for the heating assays, the Fe(III)-WS_2-PVP nanocapsules under 808 nm laser irradiation (1 W cm^{-2}, 5 min) registered an increment of approximately 14.6, 24.3, and 45.0 ˚C for concentrations of 50,100 and 200 50 μg mL^{-1}, respectively (**Figure 4a**) [34].

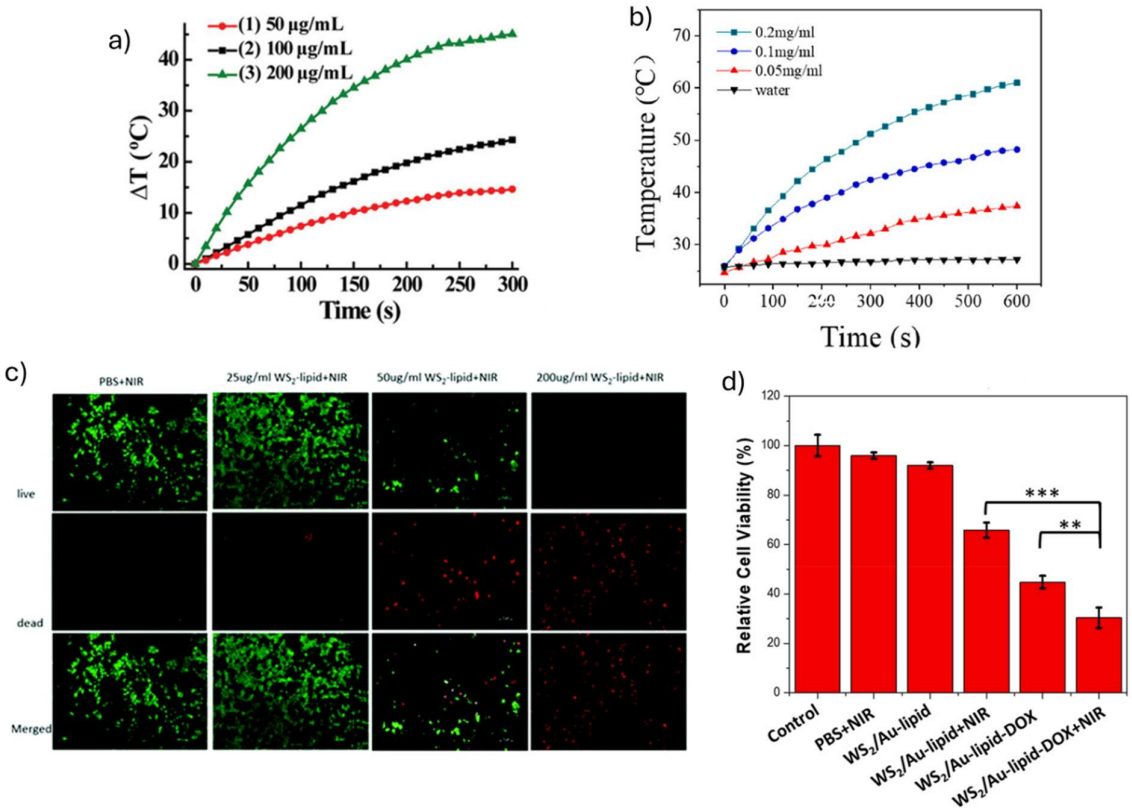

Figure 4. Tungsten disulfide-based material *in vitro* photothermal studies. (a) Fe(III)@WS_2-PVP nanocapsules (0.05-0.2 mg mL^{-1}) temperature variation under laser irradiation (808 nm, 1 W cm^{-2}, 5 min). Adapted with permission. [34] © 2019 WILEY-VCH Verlag GmbH & Co. KGaA, Weinheim. (b) Photothermal heating curves for mWS_2-lipid (0.05-0.2 mg mL^{-1}) upon irradiation (808 nm, 2 W cm^{-2} , 10 min). Adapted with permission. [36] © 2023 Elsevier B.V. All rights reserved. (c) Live/dead cell staining of MCF-7 cells after incubation with WS_2-lipid for 4 h, followed by near-infrared laser irradiation (808 nm, 2 W cm^{-2}, 10 min). Adapted with permission. [35] © The Royal Society of Chemistry 2020. (d) WS_2/Au-lipid, and WS_2/Au-lipid-DOX (DOX = 12.5 μg mL^{-1}), incubated for 24 h with MCF-7 cells, with and without laser irradiation (808 nm, 2 W cm^{-2}, 10 min). Relative cell viability determined by MTT assay. Controls were performed with MCF-7 cells alone, and PBS and NIR irradiation only. Adapted with permission. [37] © 2022 Elsevier B.V. All rights reserved. Abbreviations: DOX, doxorubicin; Fe(III)@WS_2-PVP, WS_2 conjugated with Fe(III) and modified with PVP ; m-WS_2-lipid, iron oxide modified WS_2 with lipids; PVP, Poly(vinylpyrrolidone); WS_2-lipid, WS_2 modified with lipids; WS_2/Au-lipid, Gold doped WS_2 modified with lipids.

Lipid-modified WS_2 NPs also showed the same trend when incubated with MCF-7 cells for 24 h and irradiated with an 808 nm laser (2 W cm^{-2}, 10 min). Post-treatment cell viabilities were of 43%

 doi:10.20944/preprints202410.1155.v1

and 9%, for concentrations of 50 and 200 μg mL^{-1}. After conjugation with DOX, WS_2-lipid-DOX (50 μg mL^{-1} DOX), cell viability decreased to 20%, under the same conditions (**Figure 4c)** [35]. Magnetic WS_2 functionalized with lipids, mWS_2-lipid, resulted in lower cell viability (30%, 50 μg mL^{-1}). However, DOX conjugation (50 μg mL^{-1} DOX) only slightly further reduced viability in this case (27%) [36]. Gold-doped WS_2/Au-lipid revealed to achieve higher cell viability without DOX (>90%). However, when DOX was loaded (50 μg mL^{-1}) cell viability decreased to 30% (**Figure 4d**) [37]. Furthermore, photothermal tests under 808 nm laser (2 W cm^{-2}, 10 min) irradiation increased the temperature of WS_2-lipid (200 μg mL^{-1}), mWS_2-lipid (200 μg mL^{-1}) and WS_2/Au-lipid (200 μg mL^{-1}) to 60°C, 68.1°C and 75°C (**Figure 4b**).

WID-M-FA, PEGylated WS_2 loaded with DOX and ICG, and coated with an erythrocyte membrane, was incubated with HeLa cells at a concentration of 1 μg mL^{-1} DOX and 10 μg mL^{-1} ICG. After 24 h, irradiation was performed with an 808 nm laser (1 W cm^{-2}, 5 min), with a decrease of about 30% being obtained in cell viability. A live/dead assay revealed that about 70 % of the tumor cells were killed after laser irradiation [40].

In sum, abovementioned studies generally reveal that cell viability decreases with WS_2-based materials concentration and laser power increase. Conjugation with drugs, such as DOX also can contribute to increase in vitro anticancer effectiveness.

7. In Vivo Photothermal Therapy Studies

In vivo studies have been performed to evaluate the possibility of clinical translation of the use of WS_2-based materials for cancer PTT. The main results are summarized in **Table 5**.

Table 5. *In vivo* photothermal therapy studies using tungsten disulfide-based materials.

2D material	Energy (W cm^{-2})	Time (min)	Animal model	Tumor growth	Additional outcomes	Reference
Fe (III)-WS_2-PVP-DOX	1	5	HT29 colorectal carcinoma bearing Balb/c mice	i.v. administration (250 μg mL^{-1}) Tumors volume decreased during the study (15% compared to control, 28 days after irradiation)	-	[34]
WS_2 – PEG	0.8	5	4T1 tumor bearing Balb/C mice	i.t administration (2 mg kg^{-1}, 30 min incubation) i.v. administration (20 mg kg^{-1}, 24 h incubation) Tumors were eliminated after 2 days of irradiation No tumor regrowth during the study (14 days after irradiation)	-	[28]

 doi:10.20944/preprints202410.1155.v1

WS_2-IO-MS-PEG/DOX	0.55	10	4T1 tumor bearing Balb/C mice	i.v. administration (WS_2 = 8.4 mg kg^{-1}, DOX = 7 mg kg^{-1}, 24 h) Tumors volume decreased during the study (10% compared to control, 14 days after irradiation) Tumor mass decreased after 14 days	-	[32]
WID-M-FA	1	5	HeLA tumor bearing Balb/C mice	i.v. administration (DOX = 2 mg kg^{-1}, ICG = 5 mg kg^{-1}, 24 h) Tumor was eliminated after 18 days of irradiation No changes on body weight	-	[40]
N-WS_2	0.6	10	HeLa tumor-bearing female NOD/SCID mice	i.t administration (1.2 mg mL^{-1}, 40 μL, 0 h incubation) Tumor was eliminated after 4 days of irradiation No tumor regrowth during the study (14 days after irradiation)	No changes on body weight (14 d after irradiation) Significant damage in tumor tissue (2 d after irradiation) Serum biochemistry markers on normal ranges (6, 16 d after irradiation, WBC, RBC, Hgb, HCT, platelets, MCV, MCH, MCHC)	[38]

 doi:10.20944/preprints202410.1155.v1

PEG-WS_2:Gd^{3+}	0.5	10	4T1 tumor-bearing Balb/c mice	i.v. administration (20 mg kg^{-1}, 24 h) Tumor was eliminated 12 days after irradiation	-	[39]
WS_2-lipid	2	2	4T1 breast tumor-bearing ICR mice	i.v. administration (1 mg mL^{-1}, 24 h)	-	[35]
mWS_2-lipid	1.5	5	4T1 tumor-bearing Balb/c mice	i.v. administration (2 mg mL^{-1}, 24 h) Tumors volume decreased during the study (50% compared to control, 7 days after irradiation)	No changes in body weight	[36]
WS_2/Au-lipid	1.5	5	4T1 breast tumor-bearing female Balb/c mice	i.v. administration (DOX = 150 μg), 24 h) Tumor was eliminated after 11 days of irradiation	No changes in body weight	[37]

The 4T1 tumor-bearing Balb/c mice model was administrated with 2 mg kg^{-1} WS_2–PEG intratumorously or 20 mg kg^{-1} intravenously. After 30 min, 5 min of NIR laser irradiation (808 nm, 0.8 W cm^{-2}) was performed. In both cases, the tumor was eliminated 2 days after treatment, with no sign of regrowth after 14 days (**Figure 5a**) [28]. HeLa tumor-bearing female NOD/SCID mice were intratumorously injected with N-WS_2 (1.2 mg mL^{-1}, 40 μL), and tumors were eliminated 4 days after 5 min laser irradiation (808 nm, 0.6 W cm^{-2}), with no changes in the liver, lung, and other organs being found [38]. Blood tests presented normal values for all parameters, except for white blood cells (WBC), which slightly decreased 6 days after the treatment, which could be related to the inflammation after the photothermal therapy, even though after 16 days, the values recovered to the normal range. HeLA tumor-bearing Balb/c mice were intravenously injected with WID-M-FA NPs, erythrocyte vesicle-containing WS_2 loaded with 2 mg kg^{-1} DOX and 5 mg kg^{-1} ICG. After 24 h, NIR laser irradiation (808 nm, 1 W cm^{-2}) was performed for 5 min. After 18 days, the tumor was eliminated, and no body weight changes were recorded during the experiment. Biodistribution studies revealed high tumor accumulation of WID-M-FA NPs when laser irradiation was applied (**Figure 5c**) [40]. For the 4T1 tumor-bearing Balb/c mice treated with PEG-WS_2:Gd^{3+} (i.v. injection: 20 mg kg^{-1}, 24 h) and irradiated with NIR light (808 nm, 0.5 W cm^{-2}) for 10 min, the tumor was eliminated after 12 days [39]. Fe(III)-WS_2-PVP-DOX NPs (250 μg mL^{-1}) were intravenously injected in HT29 colorectal carcinoma-bearing Balb/c mice, followed by NIR laser irradiation (808 nm, 1 W cm^{-2}) for 5 min. After 28 days, tumor volume decreased by about 15%, compared to the control group [34]. For 4T1 tumor-bearing Balb/C mice treated with WS_2-IO-MS-PEG/DOX (WS_2 = 8.4 mg kg^{-1}, DOX = 7 mg kg^{-1}, 24 h) and irradiated for 5 min with a laser (808 nm, 0.55 W cm^{-2}), tumor volume decreased 10%

 doi:10.20944/preprints202410.1155.v1

compared to control, 14 days post-treatment (**Figure 5d**) [32]. The 4T1 tumor-bearing Balb/c mice model, has been intravenously injected m-WS_2-lipid, followed by NIR laser irradiation (808 nm, 1.5 W cm^{-2}) for 5 min every 24 h. After 7 days, tumor volume growth was reduced by 50% compared to the control group (PBS), with no changes in body weight being found. For WS_2/Au-lipid-conjugated with DOX (150 μg) and exposed to 5 min NIR irradiation (808 nm, 1.5 W cm^{-2}), the tumor was eliminated after 11 days of treatment (**Figure 5b**). Overall, lipid-modified nanoparticles were more stable in water, allowing better permeation and retention in the tumor, and also increasing their photothermal conversion capacity. The combination of PTT with chemotherapy with DOX increased the anticancer effectiveness [35–37].

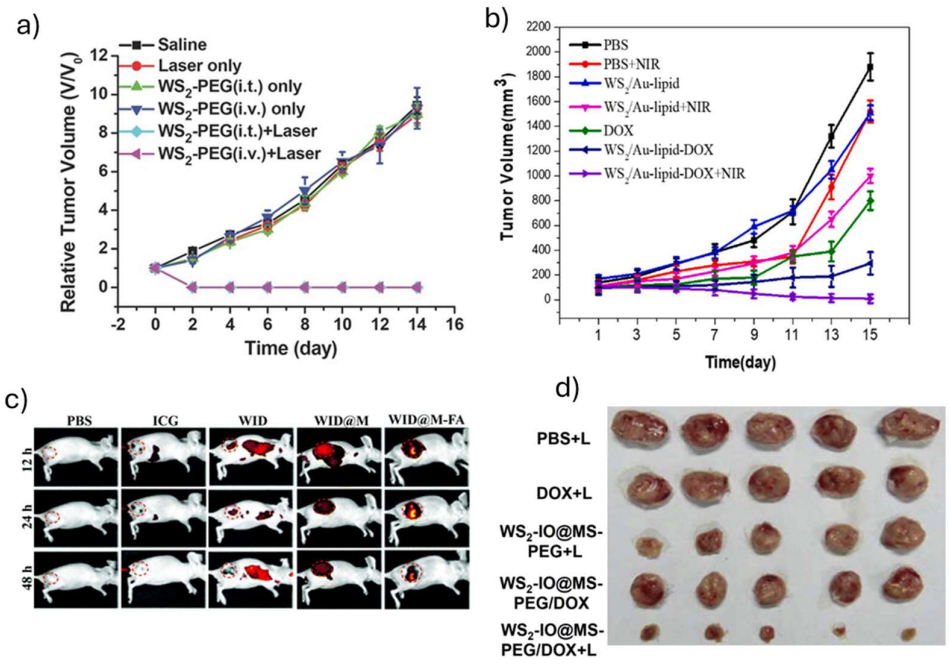

Figure 5. Tungsten disulfide-based materials *in vivo* photothermal therapy application. (a) Relative tumor volume until day 14 in a 4T1 tumor-bearing Balb/c mice model, after different treatments with WS_2-PEG administered i.t. or i.v., with or without laser irradiation (808 nm, 0.8 W cm^{-2}, 5 min). Adapted with permission. [28] © 2013 WILEY-VCH Verlag GmbH & Co. KGaA, Weinheim. (b) Volume of tumors of Balb/c mice in different treatment groups of WS_2/Au-lipid with or whitout laser irradiation (808 nm, 1.5 W cm^{-2}, 5 min). Adapted with permission. [37] © 2022 Elsevier B.V. All rights reserved. (c) Biodistribution and tumor accumulation of WID@M-FA NPs. Adapted with permission.[40] © The Royal Society of Chemistry 2020. (d) Photographs of tumors collected from mice at the end of the treatments indicated with WS_2-IO-MS-PEG/DOX (day 14), laser irradiation (808 nm, 0.55 W cm^{-2}, 10 min). Adapted with permission.[32] Copyright © 2015 Elsevier Ltd. Abbreviations: DOX, doxorubicin; ICG, indocyane green; PEG, polyethylene glycol; WID, WS_2 loaded with DOX and ICG; WID-M-FA, WS_2 loaded with DOX and ICG, and modified with an erythrocyte membrane; WS_2/Au-lipid, Gold doped WS_2 modified with lipids; WS_2-IO-MS-PEG/DOX, WS_2 functionalized with iron oxide and coated with PEG and mesoporous silica; WS_2-PEG, PEGylated WS_2.

In sum, doses of WS_2-based materials from 1-20 mg kg^{-1} have been used. Laser wavelength was 808 nm, irradiance varied from 0.55-2 W cm^{-2}, and irradiation times from 2-10 min. Many studies report a substantial tumor volume reduction or even complete tumor elimination without toxicity being found. The most successful irradiation conditions were using irradiances from 0.5-1 W cm^{-2}, for 5-10 min, and material concentrations of 1.2-20 mg kg^{-1}.

5. Conclusions

For biomedical applications, WS_2 is usually produced by ultrasound-assisted liquid phase exfoliation in water. Stability in physiological conditions is improved by surface adsorption or covalent functionalization with different molecules, such as PEG, BSA, or liposomes. Surface adsorption of the anti-cancer drug doxorubicin or gold nanoparticles has been reported to increase therapeutic effects. Usually, acidic pH and NIR laser irradiation increase drug release.

WS_2-based materials revealed to be generally biocompatible in vitro and in vivo. In vitro exposure to WS_2-based nanoparticles resulted in cell viability in the range of 80-90 %. Regarding nanoparticle-drug conjugates, cell viability follows a clear concentration dependence. For example, the cell viability of MCF-7 incubated with m-WS_2-lipid-doxorubicin decreased from 50% to 15% when increasing concentrations from 2.5 μg mL^{-1} to 50 μg mL^{-1}. In vivo, a high accumulation is observed in the spleen, liver, and tumor. However, histology results show no signs of toxicity in the liver, spleen, kidney, heart, and lungs after 48 h to 45 days of WS_2-based materials administration, even for doses as high as 20 mg kg^{-1}.

WS_2-based materials proved to be effective for cancer PTT both in vitro and in vivo. In vitro, cancer cell viability decreases with WS_2-based materials concentration and laser power increase, reaching values as low as 5-30%. Conjugation with drugs, such as doxorubicin, contributed to a further increase in in vitro anticancer effectiveness. In vivo, many studies report a substantial tumor volume reduction or even complete tumor elimination without toxicity being found. The most successful irradiation conditions were using irradiances from 0.5-1 W cm^{-2}min for 5-10 min, and material concentrations of 1.2-20 mg kg^{-1}.

Despite the promising results obtained, WS_2-based materials' long-term toxicity effects and biodegradation still need to be studied before clinical trials can be outlined.

Author Contributions: Conceptualization, A.R.L, F.D.M., J.L., and A.M.P.; methodology, A.R.L, F.D.M., J.L., and A.M.P.; validation, F.D.M., J.L., and A.M.P.; formal analysis, A.R.L, F.D.M., J.L., and A.M.P.; investigation, A.R.L, and A.M.P.; resources, F.D.M., J.L., and A.M.P.; data curation, A.R.L, and A.M.P.; writing—original draft preparation, A.R.L, and A.M.P.; writing—review and editing, A.R.L, F.D.M., J.L., and A.M.P.; visualization, A.R.L, and A.M.P.; supervision, F.D.M., J.L., and A.M.P.; project administration, F.D.M., J.L., and A.M.P.; funding acquisition, F.D.M., J.L., and A.M.P.. All authors have read and agreed to the published version of the manuscript.

Funding: This work was financially supported by ALiCE, LA/P/0045/2020 (DOI: http://doi.org/10.54499/LA/P/0045/2020); LEPABE UIDB/00511/2020 (DOI: http://doi.org/10.54499/UIDB/00511/2020); UIDP/00511/2020 (DOI: http://doi.org/10.54499/UIDP/00511/2020); and FCT project 2022.04494.PTDC - PhotoRect, using national funds through the FCT/MCTES (PIDDAC). Artur Pinto thanks the Portuguese Foundation for Science and Technology (FCT) for the financial support of his work contract through the Scientific Employment Stimulus—Individual Call—CEECIND/03908/2017 (DOI: https://doi.org/10.54499/CEECIND/03908/2017/CP1399/CT0008).

Data Availability Statement: Not applicable.

Conflicts of Interest: The authors declare no conflicts of interest.

References

1. Institute, N.C. *Global Cancer Research*. 2022; Available from: https://www.cancer.gov/research/areas/global-health.
2. Sermeus, A., et al., *Advances in radiotherapy and targeted therapies for rectal cancer.* World Journal of Gastroenterology: WJG, 2014. **20**(1): p. 1.
3. Farzam, O.R., et al., *Nanoparticles for imaging-guided photothermal therapy of colorectal cancer.* Heliyon, 2023.
4. Rodrigues, J.A. and J.H. Correia, *Photodynamic therapy for colorectal cancer: An update and a look to the future.* International Journal of Molecular Sciences, 2023. **24**(15): p. 12204.
5. Han, H.S. and K.Y. Choi, *Advances in nanomaterial-mediated photothermal cancer therapies: toward clinical applications.* Biomedicines, 2021. **9**(3): p. 305.
6. Silva, F.A., et al., *2D Nanomaterials and Their Drug Conjugates for Phototherapy and Magnetic Hyperthermia Therapy of Cancer and Infections.* Small, 2023: p. 2306137.
7. Tang, P., et al., *Thermochromism-induced temperature self-regulation and alternating photothermal nanohelix clusters for synergistic tumor chemo/photothermal therapy.* Biomaterials, 2019. **188**: p. 12-23.

8. Murugan, C., et al., *Two-dimensional cancer theranostic nanomaterials: Synthesis, surface functionalization and applications in photothermal therapy.* Journal of Controlled Release, 2019. **299**: p. 1-20.
9. Singh, S., et al., *Graphene nanomaterials: The wondering material from synthesis to applications.* Sensors International, 2022. **3**: p. 100190.
10. Zhu, Y., et al., *Graphene and graphene oxide: synthesis, properties, and applications.* Advanced materials, 2010. **22**(35): p. 3906-3924.
11. Yang, K., et al., *Graphene in mice: ultrahigh* in vivo *tumor uptake and efficient photothermal therapy.* Nano letters, 2010. **10**(9): p. 3318-3323.
12. Silva, F.A., et al., *UV-C driven reduction of nanographene oxide opens path for new applications in phototherapy.* Colloids and Surfaces B: Biointerfaces, 2024. **233**: p. 113594.
13. Murali, A., et al., *Emerging 2D nanomaterials for biomedical applications.* Materials Today, 2021. **50**: p. 276-302.
14. Hu, T., et al., *Two-dimensional nanomaterials: fascinating materials in biomedical field.* Science Bulletin, 2019. **64**(22): p. 1707-1727.
15. Liu, J., et al., *Gold nanostars decorated MnO2 nanosheets for magnetic resonance imaging and photothermal erasion of lung cancer cell.* Materials Today Communications, 2018. **16**: p. 97-104.
16. Guan, X., et al., *2D MXene nanomaterials: Synthesis, mechanism, and multifunctional applications in microwave absorption.* Small Structures, 2022. **3**(10): p. 2200102.
17. Derakhshi, M., et al., *Two-dimensional nanomaterials beyond graphene for biomedical applications.* Journal of Functional Biomaterials, 2022. **13**(1): p. 27.
18. Khandelwal, A., et al., *Phosphorene–the two-dimensional black phosphorous: Properties, synthesis and applications.* Materials Science and Engineering: B, 2017. **221**: p. 17-34.
19. Mo, S., et al., *Two-dimensional antibacterial Pd@ Ag nanosheets with a synergetic effect of plasmonic heating and Ag+ release.* Journal of materials chemistry B, 2015. **3**(30): p. 6255-6260.
20. Liu, J., et al., *Heat/pH-boosted release of 5-fluorouracil and albumin-bound paclitaxel from Cu-doped layered double hydroxide nanomedicine for synergistical chemo-photo-therapy of breast cancer.* Journal of Controlled Release, 2021. **335**: p. 49-58.
21. Rahman, M.T., et al., *Two-dimensional transition metal dichalcogenides and their composites for lab-based sensing applications: Recent progress and future outlook.* Sensors and Actuators A: Physical, 2021. **318**: p. 112517.
22. Zhou, X., H. Sun, and X. Bai, *Two-dimensional transition metal dichalcogenides: synthesis, biomedical applications and biosafety evaluation.* Frontiers in Bioengineering and Biotechnology, 2020. **8**: p. 236.
23. Gong, L., et al., *Two-dimensional transition metal dichalcogenide nanomaterials for combination cancer therapy.* Journal of materials chemistry B, 2017. **5**(10): p. 1873-1895.
24. Chou, S.S., et al., *Chemically exfoliated MoS2 as near-infrared photothermal agents.* Angewandte Chemie International Edition, 2013. **52**(15): p. 4160-4164.
25. Brent, J.R., N. Savjani, and P. O'Brien, *Synthetic approaches to two-dimensional transition metal dichalcogenide nanosheets.* Progress in Materials Science, 2017. **89**: p. 411-478.
26. Wang, S., et al., *Synthesis and biocompatibility of two-dimensional biomaterials.* Colloids and Surfaces A: Physicochemical and Engineering Aspects, 2019. **583**: p. 124004.
27. Meivita, M.P., et al., *WS2/Polyethylene Glycol Nanostructures for Ultra-Efficient MCF-7 Cancer Cell Ablation and Electrothermal Therapy.* ACS omega, 2022. **7**(27): p. 23075-23082.
28. Cheng, L., et al., *PEGylated WS2 nanosheets as a multifunctional theranostic agent for* in vivo *dual-modal CT/photoacoustic imaging guided photothermal therapy.* Advanced materials, 2014. **26**(12): p. 1886-1893.
29. Gazzi, A., et al., *Photodynamic therapy based on graphene and MXene in cancer theranostics.* Frontiers in Bioengineering and Biotechnology, 2019. **7**: p. 295.
30. Silva, F.A.L.S., et al., *2D Nanomaterials and Their Drug Conjugates for Phototherapy and Magnetic Hyperthermia Therapy of Cancer and Infections.* Small, 2023.
31. Robinson, J.T., et al., *Ultrasmall reduced graphene oxide with high near-infrared absorbance for photothermal therapy.* Journal of the American Chemical Society, 2011. **133**(17): p. 6825-6831.
32. Yang, G., et al., *Two-dimensional magnetic WS2@ Fe3O4 nanocomposite with mesoporous silica coating for drug delivery and imaging-guided therapy of cancer.* Biomaterials, 2015. **60**: p. 62-71.
33. Yi, H., et al., *Liquid exfoliated biocompatible WS 2@ BSA nanosheets with enhanced theranostic capacity.* Biomaterials Science, 2021. **9**(1): p. 148-156.
34. Wu, C., et al., *Biodegradable Fe (III)@ WS2-PVP nanocapsules for redox reaction and TME-enhanced nanocatalytic, photothermal, and chemotherapy.* Advanced Functional Materials, 2019. **29**(26): p. 1901722.
35. Xie, M., et al., *WS 2 nanosheets functionalized by biomimetic lipids with enhanced dispersibility for photothermal and chemo combination therapy.* Journal of Materials Chemistry B, 2020. **8**(11): p. 2331-2342.
36. Xie, M., et al., *Magnetic WS2 nanosheets functionalized by biomimetic lipids with enhanced dispersibility for combined photothermal and chemotherapy therapy.* Journal of Drug Delivery Science and Technology, 2023. **86**: p. 104744.
37. Li, J., et al., *Construction of WS2/Au-lipid drug delivery system for multiple combined therapy of tumor.* Journal of Drug Delivery Science and Technology, 2022. **76**: p. 103747.

 doi:10.20944/preprints202410.1155.v1

38. Liu, Q., et al., *Stable metallic 1T-WS 2 ultrathin nanosheets as a promising agent for near-infrared photothermal ablation cancer therapy.* Nano Research, 2015. **8**: p. 3982-3991.
39. Cheng, L., et al., *Bottom-up synthesis of metal-ion-doped WS2 nanoflakes for cancer theranostics.* ACS nano, 2015. **9**(11): p. 11090-11101.
40. Long, Y., et al., *PEGylated WS 2 nanodrug system with erythrocyte membrane coating for chemo/photothermal therapy of cervical cancer.* Biomaterials Science, 2020. **8**(18): p. 5088-5105.
41. Zhang, H., et al., *Recent advances of two-dimensional materials in smart drug delivery nano-systems.* Bioactive Materials, 2020. **5**(4): p. 1071-1086.
42. Martín, C., et al., *Biocompatibility and biodegradability of 2D materials: graphene and beyond.* Chemical communications, 2019. **55**(39): p. 5540-5546.
43. Iso, I., *10993–5: 2009 Biological evaluation of medical devices—part 5: tests for* in vitro *cytotoxicity*. International Organization for Standardization, Geneva, 2009. **34**.